

## Article

# Remediation of Micro-Pollution in an Alkaline Washing Solution of Fly Ash Using Simulated Exhaust Gas: Parameters and Mechanism

Lei Wang <sup>1,†</sup>, Yuemei Tang <sup>1,2,†</sup>, Yu Gong <sup>2,\*</sup>, Xiang Shao <sup>2</sup>, Xiaochen Lin <sup>2</sup> , Weili Xu <sup>2</sup>, Yifan Zhu <sup>2</sup>, Yongming Ju <sup>2,3,\*</sup>, Lili Shi <sup>2</sup> and Dorota Kołodyńska <sup>4</sup> 

<sup>1</sup> School of Environmental Science and Engineering, Nanjing Tech University, Nanjing 211816, China

<sup>2</sup> State Environmental Protection Key Laboratory of Pesticide Environmental Assessment and Pollution Control, Nanjing Institute of Environmental Sciences, Ministry of Ecology and Environment (MEE), Nanjing 210042, China

<sup>3</sup> The Key Laboratory of Water and Air Pollution Control of Guangdong Province, South China Institute of Environmental Sciences, Ministry of Ecology and Environment (MEE), Guangzhou 510655, China

<sup>4</sup> Department of Inorganic Chemistry, Faculty of Chemistry, Maria Curie-Skłodowska University, Maria Curie-Skłodowska Sq. 2, 20-031 Lublin, Poland

\* Correspondence: gongyu111@hotmail.com (Y.G.); jym@nies.org (Y.J.); Tel.: +86-25-85287087 (Y.J.)

† These authors contributed equally to this work.

**Abstract:** Currently, there is an urgent need to remediate heavy metals (HMs) and high alkalinity in the washing solution of fly ash (FA). This study investigated the remediation with simulated exhaust gases of two CO<sub>2</sub> partial pressure and revealed the removal efficiency of target pollutants, mainly including Pb ions. The results verify that under the preferred conditions of 25 °C and 15 mL/min flow rate, bubbling two kinds of simulated flue gases could efficiently remove 97.9–99.2% of Pb ions. Moreover, the initial 40 min removal of Pb ions fits in a way with a pseudo-first-order equation. Based on the thermodynamic parameters, we infer that the removal of Pb ions was a spontaneous, exothermic, and entropy-decreasing process. Furthermore, residual HMs and terminal pH after remediation of the FA washing solution basically met the regulatory threshold values of the integrated wastewater discharge standard in China (GB 8978–1996). Additionally, the particles obtained from the washing solution of FA were identified as CaCO<sub>3</sub>, which was mainly composed of vaterite and calcite crystalline. This study provides a fundamental guide for remediating multiple pollutants in the washing solution of FA and simultaneously sequestering carbon emissions from power plants and industries.

**Keywords:** carbon capture, utilization, and storage (CCUS); washing solution; municipal solid waste incineration (MSWI); fly ash; heavy metals



check for updates

**Citation:** Wang, L.; Tang, Y.; Gong, Y.; Shao, X.; Lin, X.; Xu, W.; Zhu, Y.; Ju, Y.; Shi, L.; Kołodyńska, D.

Remediation of Micro-Pollution in an Alkaline Washing Solution of Fly Ash Using Simulated Exhaust Gas:

Parameters and Mechanism.

*Sustainability* **2023**, *15*, 5873. <https://doi.org/10.3390/su15075873>

Academic Editor: Luca Di Palma

Received: 2 February 2023

Revised: 5 March 2023

Accepted: 21 March 2023

Published: 28 March 2023



**Copyright:** © 2023 by the authors. Licensee MDPI, Basel, Switzerland. This article is an open access article distributed under the terms and conditions of the Creative Commons Attribution (CC BY) license (<https://creativecommons.org/licenses/by/4.0/>).

## 1. Introduction

During rapid urbanization, municipal solid waste incineration (MSWI) has gradually and globally been selected as the most successful strategy for waste management [1–3]. However, MSWI could generate considerable hazardous alkaline fly ash (FA), which has been listed in the Chinese National Hazardous Waste Inventory (No. HW18). Presently, the stabilization/solidification of heavy metals (HMs) and the detoxification of dioxin are the main research hotspots for FA treatment. Although alkaline materials can sequester CO<sub>2</sub> gas through mineral carbonation of alkaline components [4], excessive alkaline FA is seldom applied to reduce the greenhouse gas CO<sub>2</sub> and acid exhaust gas emission [5,6]. In particular, global CO<sub>2</sub> emissions from coal plants alone have been reported to reach 10.5 Gt in 2021 [7]. Therefore, it is significant to simultaneously reduce the pollution of FA and carbon emissions from flue gases.

As one of the typical alkaline industrial wastes, FA contains a large amount of calcium oxide (CaO), indicating that FA could capture CO<sub>2</sub> with the purpose of ‘using waste to treat waste’. According to the available documents, direct carbonation of FA with CO<sub>2</sub> during the gas/solid reactions could achieve transient mass transfer of CO<sub>2</sub> and partial immobilization of HMs [8–10]. It is difficult, however, to control the carbonation ratio under conditions of high pressure and high temperature [11,12]. Moreover, Dananjayan et al. reported that in the case of the wet carbonation of coal fly ash (CFA), adoption with a water slurry of 15 as L/S ratio could achieve the maximum sequestration capacity as 50.3 g CO<sub>2</sub>/kg waste, compared to the maximum sequestration capacity of 26.3 g CO<sub>2</sub>/kg dry CFA for dry carbonation [13]. This indicates that adding H<sub>2</sub>O into the FA carbonation process could significantly increase the transfer of CO<sub>2</sub> during the slow route of dry carbonation. Thus, the carbonation of FA is mainly carried out under aqueous conditions, dominated by alkaline solution.

Wet carbonation is a major process to simultaneously achieve the washing pretreatment of FA and in controlling CO<sub>2</sub> emission, which is favored by researchers because it exhibits a wide range of advantages: simple equipment, lower energy consumption, higher carbonation efficiency, and the desalination of FA [14,15]. As for the wet carbonation reactions, much attention has been focused on the effects of particle size [16], temperature [17], pressure, liquid–solid ratio [4], time, CO<sub>2</sub> volume fraction and flow rate, pH and acid gas (e.g., SO<sub>2</sub> [18]). To recycle carbonates with high purity [19], various leaching agents, including water, acids [20–22], alkali [23] and salts [24–27], have been applied to accelerate the extraction of calcium components from alkaline waste, followed by the carbonation under two-phase gas–liquid conditions.

Our prior experiments demonstrated that washing FA could promote the dissolution of hazardous materials into the washing solution. Then, bubbling CO<sub>2</sub> into the aforementioned FA washing solution can effectively deposit the amphoteric HMs, including Pb, Zn, and Cu [28], and control the high alkalinity [29]. In addition, direct CO<sub>2</sub> capture using alkaline FA has another limitation, i.e., this process does not destroy residual dioxins and may release CO<sub>2</sub> during further pyrolysis of the carbonized FA. Our prior study used a microwave (MW)-induced pyrolysis reaction to treat FA, which had been pre-treated with phosphate-containing anionic water solution [29,30]. The results demonstrated that above 99% of dioxin in FA was effectively degraded within the pyrolysis temperature varying between 380–610 °C [31]. Therefore, we propose that the detoxification of FA should be treated in steps. For example, soluble contaminants and dioxin in FA can be separately treated by a washing pre-treatment and an MW-induced pyrolysis process.

As for the washing solution of FA, bubbling CO<sub>2</sub> exhaust gas is expected to remediate the micro-pollution and sequester CO<sub>2</sub> simultaneously. Previously, high removal efficiencies (up to 99.37–99.69%) of Zn(II), Pb(II), Cu(II), and Cr(III) have been observed in wastewater treated by fly ash–lime carbonation [32]. Furthermore, a high concentration of Ca(OH)<sub>2(aq)</sub> was prone to generating CaCO<sub>3</sub> [33] when CO<sub>2</sub> was bubbled into alkali wastewater. Meanwhile, the calcite precipitation reaction could effectively reduce the pH of alkali wastewater (e.g., CO<sub>2</sub> + 2OH<sup>−</sup> = CO<sub>3</sub><sup>2−</sup> + H<sub>2</sub>O; Ca<sup>2+</sup> + CO<sub>3</sub><sup>2−</sup> = CaCO<sub>3</sub>; ΔH<sub>298K</sub> = −178 kJ/mol [34]). The simultaneous removal mechanism of amphoteric HMs during the recycling CaCO<sub>3</sub>, however, has not been clearly elucidated due to low solubility (e.g., K<sub>sp</sub>(PbCO<sub>3</sub>) = 3.3 × 10<sup>−14</sup>, K<sub>sp</sub>(CaCO<sub>3</sub>) = 2.7 × 10<sup>−9</sup>) and complex components. Additionally, based on the available data, exhaust emissions from power plant/industrial emissions which contain CO<sub>2</sub> have been rarely applied to remediate the micro-pollution in the washing solution of FA.

In this study, the main objectives were to remediate target HMs (e.g., Pb, Cu, and Zn), neutralize the alkalinity of the washing solution of FA, and sequester CO<sub>2</sub> using simulated power plant/industrial emissions. We simulated dry-based exhaust gases of the coal-fired power plant (CFPP) and the cement/steel industry with 15% and 33% partial pressure of CO<sub>2</sub> [35], respectively. Then, we remediated the washing solution of FA with the simulated exhaust gases and revealed variations of target HM concentrations, including Pb ions

and pH values versus reaction time. Furthermore, we investigated the thermodynamics and mechanism of Pb removal. Eventually, the obtained particles were characterized in detail. This study provides fundamental guidance for the simultaneous remediation of micro-pollution in the washing solution of FA and the reduction of carbon emissions in power plants/industries.

## 2. Materials and Methods

### 2.1. Fly Ash Sample and Analysis Testing

Fly ash used in this study was collected from a MSWI facility in Suzhou, China. The furnace was equipped with an air pollution control system composed mainly of a semi-dry flue gas cleaning tower, an active carbon absorption reactor, and a bag filter. Fly ash was homogeneously mixed, further dried at 105 °C for 24 h, and eventually characterized for its chemical composition. The major elements of the original fly ash were characterized with X-ray fluorescence (XRF-1700, Shimadzu Corporation, Kyoto, Japan). XRD patterns were recorded using Cu K $\alpha$  radiation (e.g., 50 KeV, 200 mA; an X'Pert Pro diffractometer) to identify the crystal phases of the original fly ash and the precipitates (Smart Lab, Rigaku, Tokyo, Japan). Next, the morphology and composition of fly ash were characterized with field emission scanning electron microscope-energy dispersion X-ray spectroscopy (SEM-EDS, Regulus8100, Hitachi, Tokyo, Japan). The samples were loaded with gold before examination by a JSM6301 analyzer with a voltage of 15 kV and 1.5 nm resolution. The detailed characterization of the original fly ash was discussed in our previous study [33].

### 2.2. Bubbling Experiments for the Washing Solution of Fly Ash

In this study, the washing parameters of FA have been mainly selected as liquid-to-solid (L/S) ratio of 3–10 mL/g, 1 L of washing solution, 10 min of washing duration, and standard ambient temperature and pressure. After the washing process, the leachate was separated with vacuum filtration. The residual HMs and pH values in the leachate were determined using the inductively coupled plasma mass spectrometer (ICP-MS, iCAP RQ, Thermo Fisher, Waltham, MA, USA) or inductively coupled plasma optical emission spectrometer (ICP-OES, iCAP 7200, Thermo Fisher, Waltham, MA, USA) and pH meter (PHC101, HACH, Loveland, CO, USA). Finally, the washed FA was dried with a freeze-drying process (−80 °C for 24 h) for further characterization. Moreover, the industrial tail gases from the CFPP and cement/steel industries with CO<sub>2</sub> and N<sub>2</sub> (CO<sub>2</sub> partial pressure as 15% and 33%, respectively) were simulated, and the effects of gas partial pressures on element removals in the washing solution were compared. The whole apparatus is available in Figure S1. The details of the bubbling experiments were described as follows:

First, high-purity N<sub>2</sub> and high-purity CO<sub>2</sub> were connected with an electromagnetic mass flowmeter (LZB-3WB, Senlod, Nanjing, China) to control the flow rates of the two gases proportionally. Second, a gas mixing device was applied to mix thoroughly the aforementioned gases, which were further heated to the specified temperatures (e.g., 25 °C, 50 °C, and 80 °C) through a gas preheating device. Additionally, the flow rates of 10 mL/min (sccm) and 15 sccm were conducted to reveal the influence of gas flow rates on the treatment of the washing solution.

The washing solutions of FA were subjected to the bubbling system using sufficiently mixed and heated gases. The FA washing solution was placed into a special reaction vessel, in which a pH meter (continuous measurement mode) was immersed and a temperature sensor was connected to ensure a constant temperature of 25 °C. Then, the fully mixed gas of 25 °C was passed into the aforementioned reactor. When the pH value changed to the preset value (pH = 8), the supply of the simulated gas was stopped. The quantitative suspensions were removed from the reactor, accompanied by a recording of the pH and the bubbling time. The suspensions were filtered through 0.45  $\mu$ m filters, and the filtrates were further collected into 50 mL colorimetric tubes and acidified (final pH value < 2). The concentrations of residual HMs were determined by ICP-OES, and the minor elements

were quantified by ICP-MS. The above experiments were also conducted at 50 °C and 80 °C (heated gas and thermostatic water bath), respectively.

To compare the characteristics of the particles precipitated at different flow rates of gases, the bubbling processes for gas flow rates of 10, 15, 30, 45, and 61 sccm were studied. Since the partial pressure of CO<sub>2</sub> was set to 33%, the bubbling experiments using pure CO<sub>2</sub> with flow rates of 3, 4.95, 9.9, 14.85, and 20 sccm were re-performed. The process of the bubbling experiment was the same as above, and the obtained particles were free-dried (−80 °C for 24 h) for further characterization.

### 3. Results and Discussion

#### 3.1. Removal of Target Pollutants in the Washing Solution of FA

Figure 1 presents the XRD patterns, SEM images, EDS analysis, and X-ray mapping images before and after the washing pre-treatment for FA. As shown in Figure 1a, the crystalline substances in the original FA could be divided into two categories, mainly including alkali chlorides (e.g., NaCl, KCl, and CaClOH) and Ca-containing phases (e.g., CaCO<sub>3</sub>, Ca(OH)<sub>2</sub>, CaSO<sub>4</sub>, and CaClOH [36]). Based on the XRD peaks shown in Figure 1a, we infer that CaCO<sub>3</sub> could be ascribed to the natural carbonation during the storage of FA. The presences of CaSO<sub>4</sub> and CaClOH were mainly due to the adsorption of acid gases (e.g., HCl and SO<sub>3</sub>) in the exhaust gas by adding lime (Equations (1) and (2)) [37]. Moreover, the residual alkaline compounds, including CaSO<sub>4</sub>, CaCO<sub>3</sub>, Ca(OH)<sub>2</sub>, and CaClOH [13], could be further applied to sequester CO<sub>2</sub> via a carbonation reaction, indicating the potential of FA for capturing CO<sub>2</sub>. Furthermore, the composition of the original FA differed greatly compared to the washed FA. Therefore, we conclude that most soluble salts, including NaCl and KCl [38], could be removed by washing. After the water washing process, Ca(OH)<sub>2</sub> were gradually generated according to Equations (3)–(5). Based on the high XRD intensity of Ca(OH)<sub>2</sub> shown in Figure 1a, we preferred to optimize L/S to 8 mL/g for the following characterization. For comparison, the reaction in Equation (3) led to the complete disappearance of CaClOH in XRD.

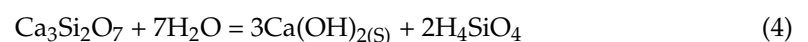
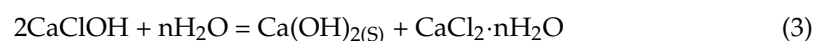
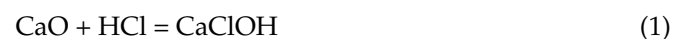
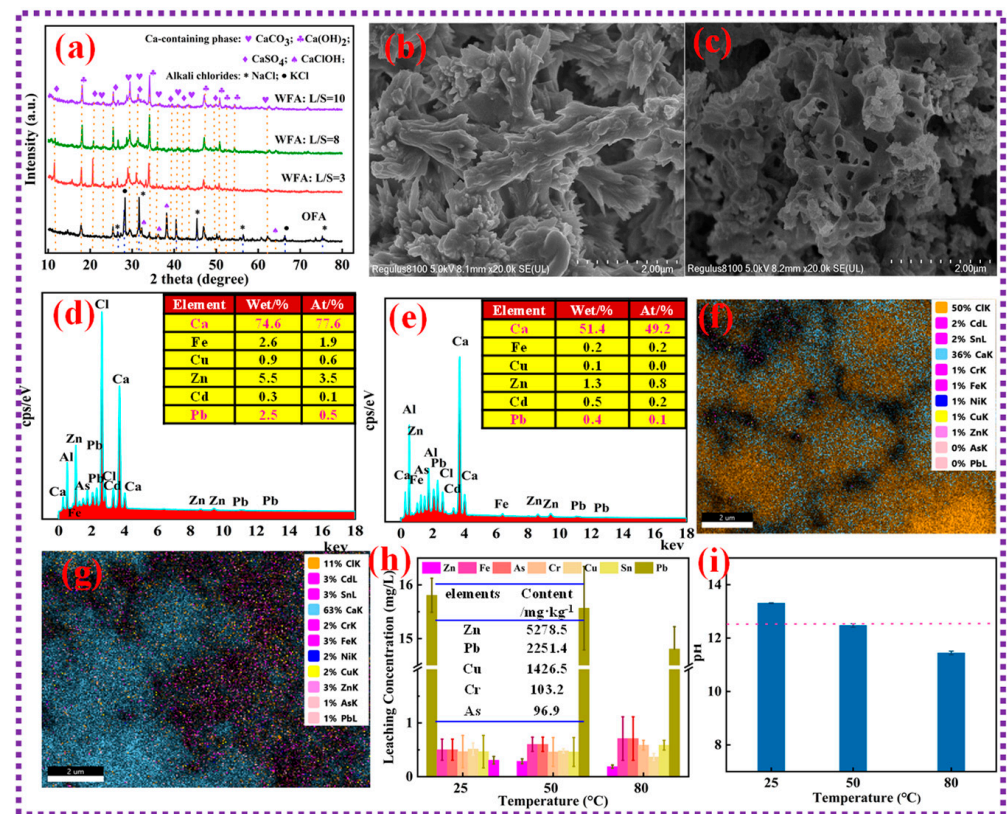


Figure 1b,c reveal the SEM variations of the original and water-washed FA. A spherical and layer-shaped structure [39] of the original FA was observed with irregular shapes compared with a dense and square structure. This indicates a significant change in the microstructures of FA after pre-treatment with washing. Moreover, the EDS spectra and X-ray mapping images shown in Figure 1d–g confirm that a washing pre-treatment could achieve the effective removal of most chlorine and soluble salts (e.g., Cl<sup>−</sup>, Na<sup>+</sup>, and K<sup>+</sup>), accompanied by the leach of HMs. Thus, the EDS spectral variations indicate that the residual concentrations of Pb, Cu, Zn, and Cd in the washed FA apparently decreased compared with the original FA. Furthermore, Figure 1h,i reveal the variations of leaching concentrations of target HMs and pH values in the washing solution. Based on the results of ICP-MS shown in the inset of Figure 1h, we conclude that fly ash had an extremely high Zn content of 5278.5 mg/kg, which is in agreement with the available document [40]. The contents of Pb, Cu, Cr, and Cd could reach up to 2251.4 mg/kg, 1426.5 mg/kg, 103.2 mg/kg, and 96.9 mg/kg, respectively. Notably, the leaching concentrations of target HMs are slightly influenced by the temperature of the washing solution. As shown in Figure 1h, the maximal leaching concentration of target HMs in washing solution at 25 °C

could reach up to 15.8 mg/L of Pb, compared with 0.64 mg/L of Cu, 0.38 mg/L of Zn, 1.37 mg/L of Cr, and 0.24 mg/L of As. This generally agrees with the prior study [41]. Furthermore, the terminal pH values of the washing solution shown in Figure 1i are basically within the range of 11.4–13.3. This indicates that the washing solution of the original FA, including Pb concentrations and pH values, did not meet the integrated wastewater discharge standard in GB 8978–1996 [42]. Thus, this emphasizes the necessity for controlling the micro-pollutions, mainly including Pb, in the washing solution of FA.



**Figure 1.** (a) The XRD patterns of the fly ash treated with different L/S; (b,c) SEM images of the original and washed fly ash; (d–g) the X-ray mapping of the original fly ash and washed fly ash (with the main element contents shown in the inset); (h) variations in leaching concentrations of target HMs; (i) final solution pH values conducted at different temperatures (with the trace elements of the original fly ash shown in the inset of (h)). Note: L/S = 8 mL/g, washing time = 10 min, washing temperature = 25 °C, 50 °C, and 80 °C, respectively.

Figure 2a–c show the removal efficiency for Pb ions and variations of pH values versus the main parameters of bubbling simulated gases into the washing solution of FA. The results show that the pH values of the washing solution slowly decreased in no more than 30 min of bubbling time, and a further increase in the bubbling time could lead to a clear downward trend in pH values. This is mainly ascribed to the high initial pH values in the washing solution of FA (approx. 13.3), which could hardly be neutralized by bubbling gases. For comparison, the carbonation reaction of 40 min could decrease the pH values of the washing solution to approximately 7. Furthermore, the effects of gas flow rates, temperatures, and different  $\text{CO}_2$  ratios on the removal efficiency of Pb ions are also recorded. As shown in Figure 2a,b, the removal efficiency of Pb ions increased from 82.2% to 97.9% when the flow rates increased from 10 to 15 sccm within 30 min of the gas bubbling process at 25 °C. In contrast, the same gas flow rates conducted at 50 °C and 80 °C had a negative influence on the removal of Pb. As for temperature, the results shown in Figure 2a–c verify that the removal efficiency of Pb significantly decreased as the carbonation temperature increased from 25 °C to 80 °C. For example, the maximum removal efficiency of Pb was up

to 97.9% at 25 °C after 29 min of bubbling. On the contrary, the removal efficiency of Pb decreased to 78.1% at 80 °C, accompanied by an increase in the bubbling time by at least 10 min (flow rate = 15 sccm, CO<sub>2</sub> ratio = 33 mol%). The above results also indicate that a higher temperature is not favorable for Pb removal in the washing solution of FA. The high temperature is detrimental to the dissolution of CO<sub>3</sub><sup>2-</sup>, which is regarded as a rate-limiting step in the carbonation process of the washing solution. Therefore, temperature could control the solubility of H<sub>2</sub>CO<sub>3</sub> [43] and further determine the carbonation for Pb removal. Additionally, Figure 2d–f present the variations of Pb versus pH values. The results shown in Figure 2d–f verify that the concentration of Pb reduced sharply within a pH of 10.25 and then decreased slowly at a temperature of 25 °C. This was consistent with the trend at other temperatures (approx. 80 °C) under the condition of 10 sccm–33 mol%. Similar phenomena could be observed in other experimental parameters (15 sccm–33 mol%, 15 sccm–15 mol%). This could be because the species distributions of H<sub>2</sub>CO<sub>3</sub> could be directly determined by the pH values of the washing solution. Consequently, the preferred flow rate of gas and temperature were optimized as 15 sccm and 25 °C, respectively.

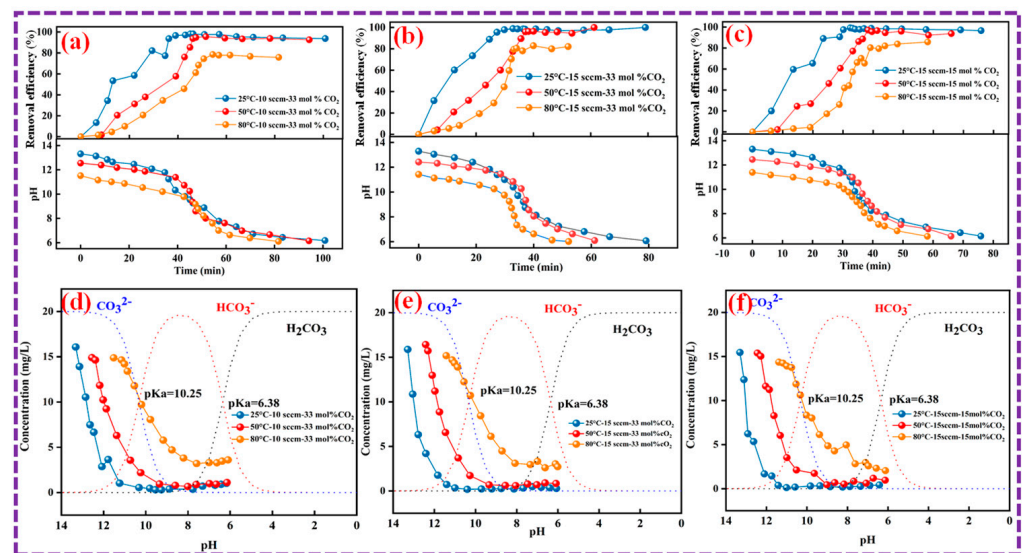


**Figure 2.** (a–c) Variations in Pb removal efficiency and solution pH values versus bubbling time of simulated exhaust gas; (d–f) variations in Pb concentration versus solution pH values (the dotted lines represent the species distributions of carbonates in the aqueous solution). Note: L/S = 8 mL/g, washing time = 10 min, washing temperature = 25 °C, 50 °C, and 80 °C, respectively; gas flow rates of 10 and 15 sccm, CO<sub>2</sub> partial pressure = 15 mol% and 33 mol%.

Under the preferred condition of 25 °C and 15 sccm gas flow rate, two simulated flue gases could significantly remove 97.9–99.2% of Pb (in Figure 2b,c). Furthermore, the maximum removal efficiency of Zn (99%) and Cu (81%) could also be observed under the same conditions (Figure S2). However, the removal efficiency of Cr and As showed no obvious patterns (Figure S2). After the bubbling treatment, the residual Pb concentration of 0.34 mg/L, as well as terminal pH in the washing solution of FA, met the regulatory standard of integrated wastewater discharge standard in GB 8978–1996 [42] (e.g., Pb: 1.0 mg/L, pH: 6–8). Therefore, it is feasible to use flue gas emitted from the CFPP and cement/steel industries to remediate the micro-pollutions in the washing solution of FA.

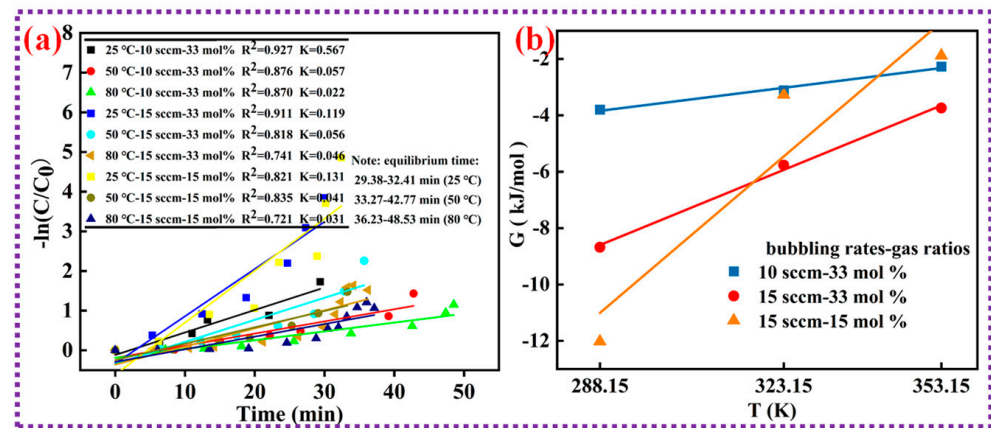
### 3.2. Kinetics Study Analysis

Figure 3a presents the variations of Pb ions concentrations versus the contact time. The results in Figure 3a reveal that within the initial 40 min of reaction, the removal of Pb ions basically fit with a pseudo-first-order kinetics model described in Equation (6). Furthermore, the maximal kinetic constant shown in the inset of Figure 3a was calculated as  $1.31 \times 10^{-1} \text{ min}^{-1}$  under the preferred conditions of 25 °C, and 15 sccm–15 mol% CO<sub>2</sub>.

Moreover, the kinetic constants of Pb ions decreased with increasing reaction temperature. For example, the maximal kinetic constants of Pb ions were classified as follows:  $1.3 \times 10^{-1} \text{ min}^{-1}$  (at  $25^\circ\text{C}$ )  $> 4.1 \times 10^{-2} \text{ min}^{-1}$  (at  $50^\circ\text{C}$ )  $> 3.1 \times 10^{-2} \text{ min}^{-1}$  (at  $80^\circ\text{C}$ ). This has also coincided with the results shown in Figure 2d–f, which presents Pb ions' variations versus pH values.

$$\ln\left(\frac{C_t}{C_0}\right) = -k_{obs} \times t \quad (6)$$

where  $C_t$  and  $C_0$  are the concentrations of Pb (mg/L) after a reaction time of  $t$  and 0 (min), respectively;  $k$  is the rate constant ( $\text{min}^{-1}$ ) of the pseudo-first-order kinetics equation, and  $t$  is the reaction time (min).



**Figure 3.** (a)  $\ln(c/c_0)$  versus bubbling time of simulated gas (with the kinetic constant of linear fitting pseudo-first-order equation of Pb shown in the inset); (b) the plot of  $\Delta G^0$  versus  $T$ . Note:  $L/S = 8 \text{ mL/g}$ , washing time = 10 min, washing temperature =  $25^\circ\text{C}$ ,  $50^\circ\text{C}$ , and  $80^\circ\text{C}$ , respectively.

To explore the thermodynamic parameters for the carbonation process, free energy change ( $\Delta G^0$ ), enthalpy ( $\Delta H^0$ ), and entropy change ( $\Delta S^0$ ) were calculated by the van 't Hoff equations shown in Equations (7)–(9) [44].

$$\ln K_D = \frac{\Delta S^0}{R} - \frac{\Delta H^0}{RT} \quad (7)$$

$$K_D = \frac{C_0 - C_e}{C_e} \quad (8)$$

$$\Delta G^0 = \Delta H^0 - T\Delta S^0 \quad (9)$$

where  $R$  is the universal gas constant ( $8.314 \text{ J mol}^{-1} \text{ K}^{-1}$ ),  $T$  is the absolute temperature (K), and  $K_D$  (L/mol) is the distribution coefficient at different temperature levels.  $K_D$  (mL/g),  $\Delta S^0$  [J/(mol K)], and  $\Delta H^0$  (kJ/mol) represent the reaction coefficient, the standard entropy, and the standard enthalpy, respectively.  $C_0$  and  $C_t$  (mg/L) are the concentrations of Pb at times 0 and  $t$ . The change in enthalpy ( $\Delta H^0$  in kJ/mol) and entropy ( $\Delta S^0$  in J/molK) could be calculated from linear coefficients using van 't Hoff's equation.

Figure 3b shows the plot of  $\Delta G^0$  versus reaction temperature within 298.15–353.15 K. As shown in Table 1, we could determine that for removing Pb ions,  $\Delta G^0$ ,  $\Delta H^0$ , and  $\Delta S^0$  are negative, negative, and negative, respectively. This indicates that the removal of Pb ions was a spontaneous, exothermic, and entropy-decreasing process. The absolute  $\Delta G^0$  values increased with increasing reaction temperature. This could be because of bubbling  $\text{CO}_2$  into the FA washing solution and the precipitation of deposits of lead and calcium carbonates. This could apparently decrease the level of disorder and randomness at the gas/solution interface. More exploration will be conducted in the following section.

**Table 1.** Thermodynamic parameters during the carbonation process (at 25 °C, 50 °C, and 80 °C, respectively).

Cations	Temp.	Rates (sccm)	CO <sub>2</sub> % Ratio	K <sub>d</sub>	ΔG <sup>0</sup> (kJ/mol)		
Pb(II)	25 °C	10	33	4.622	−3.795		
		15	15	127.833	−12.024		
		15	33	45.706	−8.680		
		10	33	3.185	−3.113		
		15	15	3.369	−3.264		
		15	33	8.547	−5.764		
	50 °C	10	33	2.166	−2.269		
		15	15	1.895	−1.877		
		15	33	3.572	−3.738		
		25 °C	10	33	−10.571	−23	0.989
		50 °C	15	15	−30.568	−76	0.997
		80 °C	15	33	−56.742	−158	0.881

### 3.3. Carbonation Mechanism

To elucidate the Pb precipitation behaviors in the washing solution system during the carbonation process (e.g., Pb<sup>2+</sup> and CO<sub>3</sub><sup>2−</sup>), we adopted the Visual MINTEQ (ver.3) to conduct the equilibrium calculations and examine the potential speciation distribution and saturation indices (SIs) versus different pH values [45]. Figure 4a–c reveal the main speciation distribution of Pb ions during the carbonation process. As shown in Figure 4a–c, the removal of Pb ions was due to the lower pH of the solution induced by bubbling CO<sub>2</sub>, accompanied by a series of changes in the chemistry and mineralogy [33]. The carbonation process occurred mainly via two consecutive steps: the solubility of Pb ions against low solution pH [46] and the transformation of Pb hydroxides into Pb carbonates. For example, Pb(OH)<sub>3</sub><sup>−</sup> ions were significant species of Pb ions in the washing solution under strongly alkaline conditions (e.g., pH > 12). As the dissolution of CO<sub>2</sub> led to a decrease in pH [47] (e.g., pH decreased from 13.3 to 9.5), Pb(OH)<sub>3</sub><sup>−</sup> ions gradually transformed into Pb(OH)<sub>2(aq)</sub> and Pb(OH)<sup>−</sup>. The aforementioned process was accompanied by the increases of Pb<sup>2+</sup> and CO<sub>3</sub><sup>2−</sup> ions in the washing solution (2Pb(OH)<sub>3</sub><sup>−</sup> + H<sub>2</sub>CO<sub>3(aq)</sub> = 2Pb(OH)<sub>2(aq)</sub> + CO<sub>3</sub><sup>2−</sup>; 2Pb(OH)<sub>2</sub> + H<sub>2</sub>CO<sub>3(aq)</sub> = 2Pb(OH)<sup>+</sup> + CO<sub>3</sub><sup>2−</sup>; 2Pb(OH)<sup>+</sup> + H<sub>2</sub>CO<sub>3(aq)</sub> = 2Pb<sup>2+</sup> + CO<sub>3</sub><sup>2−</sup>). Furthermore, Pb hydroxides could be further transformed into PbCO<sub>3</sub> due to excessive carbonate ions (Pb(OH)<sub>2(aq)</sub> + H<sub>2</sub>CO<sub>3(aq)</sub> = PbCO<sub>3(s)</sub> + 2H<sub>2</sub>O; Pb<sup>2+</sup> + CO<sub>3</sub><sup>2−</sup> = PbCO<sub>3(s)</sub>). Furthermore, the EDS images shown in Figure 4d–f verify that the components of white precipitants mainly included Ca element (e.g., 93.5–96.3 wt%) as well as Pb element (e.g., 1.9–3.3 wt%), in addition to the slight residual amounts of Al, Fe, As, and Zn elements. Furthermore, the variations of the SEM images shown in the insets of Figure 4d–f verify that the rectangular particles of precipitants gradually transformed into circular particles as the bubbling rates of CO<sub>2</sub> increased. Based on the classical nucleation and growth theory, we could conclude that CaCO<sub>3</sub> particles originate with the nucleation in a supersaturated solution and further grow into microcrystals [48]. For example, the relatively high nucleation rate could result in a small size of the obtained CaCO<sub>3</sub> shown in Equations (10) and (11) [49] and the supersaturation ratio (S) in the interface is expressed as in Equation (12).

$$r = \frac{2\gamma v}{KT \ln S} \quad (10)$$

$$J = A \exp \left[ -16\gamma^3 v^2 \pi / 3 K^3 T^2 (\ln S)^2 \right] \quad (11)$$

$$S = \sqrt{\frac{\alpha_{\text{CO}_3^{2-}} + \alpha_{\text{Ca}^{2+}}}{K_{sp}}} \quad (12)$$

where  $r$  is the radius of the critical nucleus,  $\gamma$  is interfacial free energy,  $v$  is the volume of a molecule inside the nucleus,  $K$  and  $T$  are Boltzmann constant and absolute temperature, and  $J$  is the nucleation rate, respectively;  $K_{sp}$  is the thermodynamic constant of  $\text{CaCO}_3$  and  $\alpha$  is ionic activity coefficient [50].

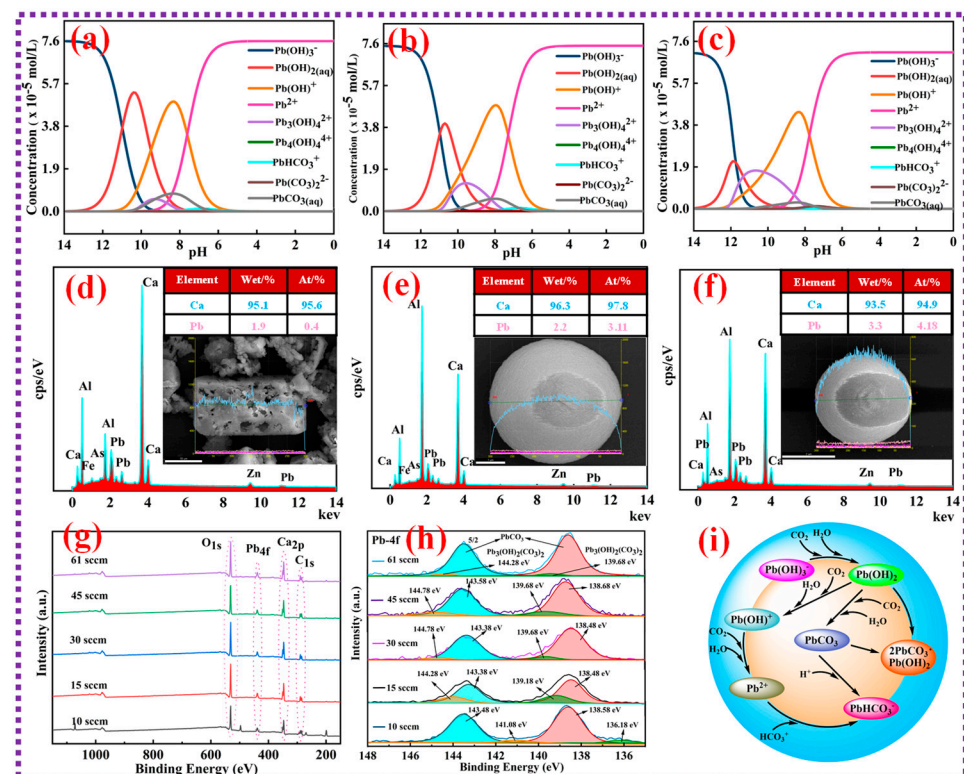


**Figure 4.** (a–c) Variations in Pb species versus pH values of the washing solution in the binary system (Pb,  $\text{CO}_3^{2-}$ ); (d–f) linear sweep of the EDS spectra for Ca and Pb elements in the selected area of  $\text{CaCO}_3$  purged with different  $\text{CO}_2$  bubbling rates (10, 15 and 30 sccm); (g,h) full scan and Pb 4f of the XPS analysis for  $\text{CaCO}_3$  samples purged with different  $\text{CO}_2$  bubbling rates; (i) the removal mechanism of Pb during the  $\text{CO}_2$  bubbling process. Note L/S = 8 mL/g, washing time = 10 min, washing temperature = 25 °C; bubbling experiments:  $\text{CO}_2$  ratio as 33%,  $\text{CO}_2$  flow rates of 10, 15, 30, 45, and 61 sccm, respectively.

Figure 4g,h compare the XPS spectral variations of precipitants. The XPS spectra show that binding energies (BEs) at 138.45 and 143.38 eV for Pb 4f doublet peaks corresponded to  $\text{PbCO}_3$  [51]. Furthermore, the BE at 144.78 and 139.68 eV were attributed to  $\text{Pb}_3(\text{CO}_3)_2(\text{OH})_2$  [52]. We infer that the co-precipitation of  $\text{PbCO}_3$  and  $\text{Pb}(\text{OH})_2$  at high alkalinity led to the generation of the aforementioned  $\text{Pb}_3(\text{CO}_3)_2(\text{OH})_2$ . Furthermore, the XPS spectra in Figure 4g,h coincided with the EDS images in Figure 4d–f, verifying the co-existence of Pb and calcium on the surface of precipitants. Furthermore,  $\text{PbCO}_3$  was mainly generated with the  $\text{CO}_2$  bubbling process, disrupting the equilibrium of the Pb complex in the alkaline washing solutions of FA. A series of carbonate precipitation processes have been proposed in Figure 4i. This indicates that the washing solution of FA has a significant capacity for  $\text{CO}_2$  capture, making it a promising candidate for efficient  $\text{CO}_2$  capture.

Table 2 summarizes the main parameters (e.g., alkaline waste source, HMs solidification, carbonation efficiency, and obtained  $\text{CaCO}_3$ ) in available carbonation processes documented with alkaline residues as feedstocks. Based on the comparisons shown in Table 2, we ascribe the different variations of carbonation capacity for alkaline solid waste to

different residue CaO contents in the alkaline solid waste. In addition, the state-of-the-art carbon capture, utilization, and storage (CCUS) techniques focus on mineral carbonation mainly via gas–solid [8,13,53] or gas–liquid–solid [36,37,54–58] processes. To our best knowledge, gas–liquid–solid reactions of CO<sub>2</sub> with fly ash could achieve rapid transient mass transfer compared with gas–solid reactions under high pressure and high-temperature conditions [27]. However, the newly adopted thermal detoxification of dioxin in FA, including a microwave-initiated thermal process [29], could destroy the mineral carbonation and lead to the release of CO<sub>2</sub>. For comparison, bubbling the pure CO<sub>2</sub> or simulated fuel gas in effluent could theoretically remove the residual HMs, and neutralize the alkalinity [28,41,59] in an aqueous solution. Meanwhile, the obtained mineral carbonate generated from bubbling the pure CO<sub>2</sub> could also be utilized for further purification of wastewater. Currently, indirect carbonation is an important process to achieve CO<sub>2</sub> storage and recover CaCO<sub>3</sub>. It focuses on using various leaching agents, such as acids [21], alkalis, and salts [24–26,60], to maximize the extraction of calcium components from the alkaline waste and produce high purity CaCO<sub>3</sub> with specific shapes.

**Table 2.** Comparison of carbonation parameters reported in the available documents associated with alkaline solid waste.

Entry	System	CaO Fraction (wt %)	Reaction Parameters	Solidification Efficiency	CO <sub>2</sub> Sequestration Efficiency **	Obtained CaCO <sub>3</sub>	Ref.
Gas–liquid–solid	MSWI FA–CO <sub>2</sub> –water (China)	CaO: 38.8%,	Dry ash and ash with 20% H <sub>2</sub> O; CO <sub>2</sub> content: 10%, 50%, 100%; Time: 2 h	Pb: 40% (final pH: 11)	3% (w/w) CO <sub>2</sub>	NA	[54]
	Coal FA–CO <sub>2</sub> –water (Australia)	CaO: 12.5–24.8%	P <sub>CO<sub>2</sub></sub> : 3 MPa; T: 20–80 °C; L/S ratios of 0.1–0.5	NA	27.05 kg CO <sub>2</sub> /t FA	NA	[55]
	Circulating fluid bed (CFB) FA–CO <sub>2</sub> –steam addition (China)	CaO: 28.42%,	T: 300–800 °C; CO <sub>2</sub> content: 5%, 10%, 15%, 20%, 100% (vol%); H <sub>2</sub> O content: 5%, 10%, 20%; Time: 1 h	NA	60 g CO <sub>2</sub> /kg FA (28.74%)	NA	[56]
	Coal FA–Supercritical CO <sub>2</sub> coupled with mechanical force–water (China)	CaO: 25.8 wt %,	T: 20–80 °C; P <sub>CO<sub>2</sub></sub> : 1–8 MPa; L/S = 1–300 mL/g; Time: 1–25 h; Stirring rate: 100–800 rpm; L/S = 1–300 mL/g	Pb: 43.4%, Cr: 98%, Cd: 60.3%	42.3 mg CO <sub>2</sub> /kg FA (1 MPa); 54 mg CO <sub>2</sub> /kg FA (8 MPa)	NA	[57]
	MSWI FA–oxy–fuel combustion flue gas–calcium carbonate oligomer regulation–water (China)	CaO: 47.3% *	T: 20 °C; P <sub>CO<sub>2</sub></sub> : 0.1 MPa; L/S = 10 L/kg; Flow rate: 200 mL/min; Time: 60 min; Stirring rate: 600 rpm	Pb: 100%, Cu: 91.3%, Zn: 99.1%	13.8%	C	[58]
	FA washing solution–CO <sub>2</sub> (China)	CaO: 53 wt % (FA)	Room temperature; Stirring rate: 63 rpm; Flow rate: 10 mL/min	Pb: 99%, Cu: 95%, Zn: 96%	NA	NA	[59]
	Electric arc furnace steelmaking slags–CO <sub>2</sub> –NH <sub>4</sub> Cl (China)	CaO: 39.04 wt %	T: 12–65 °C; L/S = 20 mL/g; MW irradiation = 90–270 W	NA	NA	C+V	[60]
	MSWI FA–simulated exhaust gas (China)	NA	T: 25–80 °C; L/S = 8 mL/g; Flow rates: 10, 15, 30, 45, and 61 sccm	Pb: 97.9–99.2% (final pH: 6–8)	NA	C+V	This study

\* These data were calculated with the Ca fraction in the corresponding literature; \*\* Carbonation efficiency: the percentage of calcium in the FA/leachate/dust/slag converted into carbonates; FA: Fly ash; NA: not available; C: calcite CaCO<sub>3</sub>, V: vaterite CaCO<sub>3</sub>, C+V: mixture of calcite and vaterite CaCO<sub>3</sub>.

### 3.4. Characteristics of Obtained Particle

Figure 5a presents the XRD patterns of obtained particles. By comparing with the aforementioned two reference patterns of CaCO<sub>3</sub>, we infer that the obtained particles were mainly composed of calcite (JCPDS No. 47–1743) and vaterite (JCPDS No. 33–0268) microcrystalline. The SEM images presented in Figure 5b,c further show that the obtained

particles were aggregates of smaller units. With increasing flow rates of CO<sub>2</sub>, the ratios of vaterite to calcite gradually increased, but suddenly dropped at the highest flow rate (Figure 5d). Previously, the polymorph formation of CaCO<sub>3</sub> has been reported to be highly influenced by the precipitation conditions, including pH, supersaturation, temperature, and additives [61]. In this study, different CO<sub>2</sub> flow rates may affect both pH and supersaturation in the solution. Thus, the transformation between vaterite and calcite of CaCO<sub>3</sub> could be ascribed to a result of compound effects [61,62]. More importantly, vaterite has been reported to excel in removing toxic metal ions, including Pb<sup>2+</sup> [63,64]. Correspondingly, the vaterite contents were higher under 15 sccm flow rate of CO<sub>2</sub> than 10 sccm (Figure 5b). As shown in Figure 2a,b, we found that under the simulated flue gas at 15 sccm, the removal efficiency of Pb ions was better compared with that at 10 sccm. In the future, the gas flow rates of 30 sccm and 45 sccm should also be considered for the HMs removal in the washing solution.

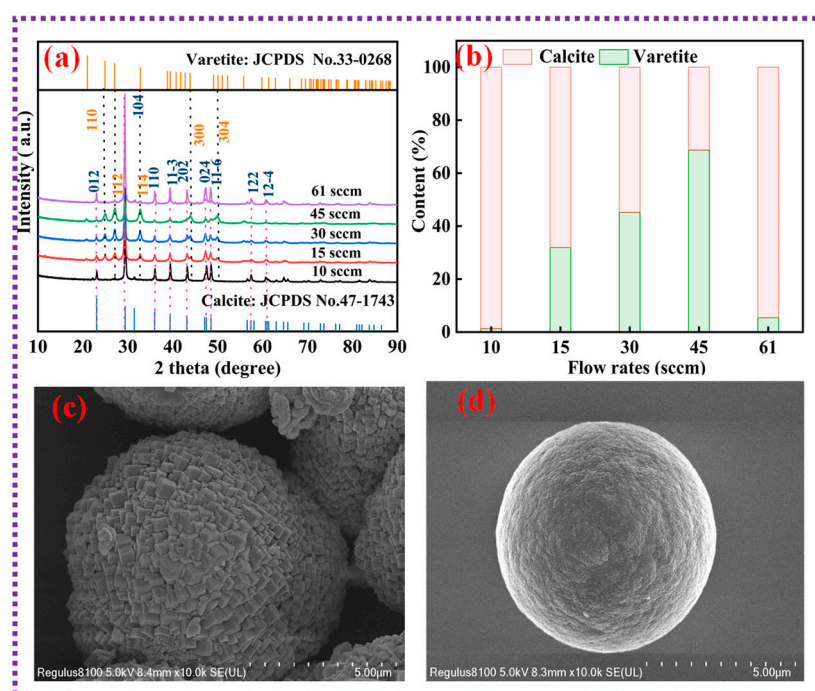


**Figure 5.** (a) The XRD patterns of particles obtained at different CO<sub>2</sub> flow rates; (b) Relative contents of vaterite and calcite obtained at different CO<sub>2</sub> flow rates; (c,d) The SEM images of aggregates composed of calcite and vaterite, respectively. Note: CO<sub>2</sub> flow rates of 10, 15, 30, 45 and 61 sccm; L/S = 8 mL/g, washing time = 10 min, washing temperature = 25 °C.

The XRD patterns and SEM images indicate that the obtained particles were mainly composed of vaterite and calcite of CaCO<sub>3</sub>. The EDS images in Figure 4d–f and the XPS spectra in Figure 4h verify the existence of a small amount of Pb in these obtained particles. Therefore, the toxicity of obtained particles needed to be evaluated, and the associated experiments were described in the Supplementary Materials. The acute toxicity experiment demonstrates that the mortality rates of zebrafish were 0% after exposure to obtained particles for 24 h, 48 h, 72 h, and 96 h, respectively. Given that zebrafish is an excellent model animal for human health research [65], we infer that the obtained particles from the washing solution are safe for further application. Moreover, we used 50 mg of obtained particles for the adsorption of 50 mL Congo red dye (initial concentration: 10 mg/L, 15 mg/L, 20 mg/L, and 30 mg/L, respectively), which was conducted in a thermostatic oscillator (e.g., 150 rpm, 24 h). The results shown in Figure S3 verify that obtained CaCO<sub>3</sub> particles could function as promising adsorbents.

#### 4. Conclusions

The simulated exhaust gases of CFPP and cement/steel industry could achieve the remediation of micro-pollution, including Pb and alkalinity in the washing solution for MSWI fly ash (e.g., Pb: 14.8 mg/L–15.8 mg/L; solution pH: 12.8–13.6). After the bubbling treatment with simulated exhaust gases in the washing solution, the residual concentration of HMs, including Pb ions and terminal pH, basically met the regulatory threshold values of integrated wastewater discharge standard in China (Pb: 1.0 mg/L, pH = 6–9). The removal of Pb ions was a spontaneous, exothermic, and entropy-decreasing process, and the proposed removal mechanism was ascribed to the generation of  $\text{PbCO}_3$  and  $\text{Pb}_3(\text{OH})_2(\text{CO}_3)_2$ . The obtained  $\text{CaCO}_3$  was proved non-toxic by acute toxicity test and showed a quick adsorption performance of Congo red dye. This study demonstrates the possibility of simulated  $\text{CO}_2$  exhaust gas to remediate micro-pollution of FA washing solution, and provides a theoretical basis for the reuse of real exhaust gas containing  $\text{CO}_2$ . In the context of carbon neutrality and emission peak, the effective utilization of exhaust gas containing  $\text{CO}_2$  can reduce the HM pollution of FA washing solution, sequester  $\text{CO}_2$ , and recover  $\text{CaCO}_3$ .

**Supplementary Materials:** The following supporting information can be downloaded at: <https://www.mdpi.com/article/10.3390/su15075873/s1>, Figure S1: Schematic process flow for MSWI fly ash (FA) carbonation; Figure S2: (a–c) Variations in Cu removal efficiency versus bubbling time of simulated exhaust gas; (d–f) variations in Zn removal efficiency versus bubbling time of simulated exhaust gas; (g–i) variations in As removal efficiency versus bubbling time of simulated exhaust gas; (j–l) variations in Cr removal efficiency versus bubbling time of simulated exhaust gas. Note: the preferred ratio between liquid and solid, L/S = 8 mL/g, washing time = 10 min, washing temperature = 25 °C, 50 °C and 80 °C, respectively. The  $\text{CO}_2$  proportions in simulated exhaust gases were 15 mol% and 33 mol%, and flow rates were selected as 10 sccm and 15 sccm, respectively; Figure S3: Removal of Congo red dye by particles obtained under  $\text{CO}_2$  aeration with different flow rates (10, 15, 30, 45, and 61 sccm).

**Author Contributions:** Conceptualization, Y.J.; Methodology, L.W.; Validation, Y.T.; Formal analysis, Y.G.; Investigation, Y.T.; Resources, Y.J.; Data curation, Y.T.; Writing—original draft preparation, Y.T.; Funding acquisition, Y.J.; Visualization, Y.T.; Writing—review and editing, X.L., W.X., Y.Z., Y.G. and Y.J.; Supervision, Y.J., X.S., D.K., Y.G. and L.S. All authors have read and agreed to the published version of the manuscript.

**Funding:** The authors acknowledge the fundings provided by the National Key Research and Development Program of China (Grant No.: 2019YFE0111100), the Central Scientific Research Projects for Public Welfare Research Institutes (Grant No.: GYZX210301), and the National Natural Science Foundation of China (Grant No.: 52170137).

**Informed Consent Statement:** Not applicable.

**Data Availability Statement:** Not applicable.

**Acknowledgments:** We sincerely thank the editors and the four anonymous reviewers for their constructive suggestions and comments.

**Conflicts of Interest:** The authors declare that they have no conflict of interest.

#### References

1. Wang, L.; Zhang, Y.; Chen, L.; Guo, B.; Tan, Y.; Sasaki, K.; Tsang, D.C.W. Designing Novel Magnesium Oxysulfate Cement for Stabilization/Solidification of Municipal Solid Waste Incineration Fly Ash. *J. Hazard. Mater.* **2022**, *423*, 127025. [[CrossRef](#)] [[PubMed](#)]
2. Chen, Z.; Zhang, S.; Lin, X.; Li, X. Decomposition and Reformation Pathways of PCDD/Fs during Thermal Treatment of Municipal Solid Waste Incineration Fly Ash. *J. Hazard. Mater.* **2020**, *394*, 122526. [[CrossRef](#)] [[PubMed](#)]
3. Le, N.H.; Razakamanantsoa, A.; Nguyen, M.L.; Phan, V.T.; Dao, P.L.; Nguyen, D.H. Evaluation of Physicochemical and Hydromechanical Properties of MSWI Bottom Ash for Road Construction. *Waste Manag.* **2018**, *80*, 168–174. [[CrossRef](#)] [[PubMed](#)]
4. Qin, J.; Zhang, Y.; Yi, Y.; Fang, M. Carbonation of Municipal Solid Waste Gasification Fly Ash: Effects of Pre-Washing and Treatment Period on Carbon Capture and Heavy Metal Immobilization. *Environ. Pollut.* **2022**, *308*, 119662. [[CrossRef](#)]
5. Jozewicz, W.; Chang, J.C.S.; Sedman, C.B. Bench-Scale Evaluation of Calcium Sorbents for Acid Gas Emission Control. *Environ. Prog.* **1990**, *9*, 137–142. [[CrossRef](#)]

6. Zhang, T.A.; Zhao, H.; Liu, Y.; Dou, Z.; Lv, G.; Zhao, Q.; Li, Y. Recent Advances in Carbon Dioxide Mineralization to Nano-Size Calcium Carbonate Utilizing Wastewater. In *Energy Technology 2014*; Wang, C.W., de Bakker, J., Belt, C.K., Jha, A., Neelameggham, N.R., Pati, S., Prentice, L.H., Tranell, G., Brinkman, K.S., Eds.; John Wiley & Sons, Inc.: Hoboken, NJ, USA, 2014; pp. 103–110. [CrossRef]
7. IEA. Global Energy Review: CO<sub>2</sub> Emissions in 2021—Analysis. Available online: <https://www.iea.org/reports/global-energy-review-co2-emissions-in-2021-2> (accessed on 18 December 2022).
8. Gu, Q.; Wang, T.; Wu, W.; Wang, D.; Jin, B. Influence of Pretreatments on Accelerated Dry Carbonation of MSWI Fly Ash under Medium Temperatures. *Chem. Eng. J.* **2021**, *414*, 128756. [CrossRef]
9. Zdeb, J.; Howaniec, N.; Smolinski, A. Experimental Study on Combined Valorization of Bituminous Coal Derived Fluidized Bed Fly Ash and Carbon Dioxide from Energy Sector. *Energy* **2023**, *265*, 126367. [CrossRef]
10. Yuan, Q.; Zhang, Y.; Wang, T.; Wang, J. Characterization of Heavy Metals in Fly Ash Stabilized by Carbonation with Supercritical CO<sub>2</sub> Coupling Mechanical Force. *J. CO<sub>2</sub> Util.* **2023**, *67*, 102308. [CrossRef]
11. Abe, M.; Tanaka, S.; Noguchi, M.; Yamasaki, A. Investigation of Mineral Carbonation with Direct Bubbling into Concrete Sludge. *ACS Omega* **2021**, *6*, 15564–15571. [CrossRef]
12. Liu, W.; Teng, L.; Rohani, S.; Qin, Z.; Zhao, B.; Xu, C.C.; Ren, S.; Liu, Q.; Liang, B. CO<sub>2</sub> Mineral Carbonation Using Industrial Solid Wastes: A Review of Recent Developments. *Chem. Eng. J.* **2021**, *416*, 129093. [CrossRef]
13. Tamilselvi Dananjayan, R.R.; Kandasamy, P.; Andimuthu, R. Direct Mineral Carbonation of Coal Fly Ash for CO<sub>2</sub> Sequestration. *J. Clean. Prod.* **2016**, *112*, 4173–4182. [CrossRef]
14. Chen, J.; Fu, C.; Mao, T.; Shen, Y.; Li, M.; Lin, X.; Li, X.; Yan, J. Study on the Accelerated Carbonation of MSWI Fly Ash under Ultrasonic Excitation: CO<sub>2</sub> Capture, Heavy Metals Solidification, Mechanism and Geochemical Modelling. *Chem. Eng. J.* **2022**, *450*, 138418. [CrossRef]
15. Chen, W.; Wang, Y.; Sun, Y.; Fang, G.; Li, Y. Release of Soluble Ions and Heavy Metal during Fly Ash Washing by Deionized Water and Sodium Carbonate Solution. *Chemosphere* **2022**, *307*, 135860. [CrossRef] [PubMed]
16. Chen, J.; Shen, Y.; Chen, Z.; Fu, C.; Li, M.; Mao, T.; Xu, R.; Lin, X.; Li, X.; Yan, J. Accelerated Carbonation of Ball-Milling Modified MSWI Fly Ash: Migration and Stabilization of Heavy Metals. *J. Environ. Chem. Eng.* **2023**, *11*, 109396. [CrossRef]
17. Ji, L.; Yu, H.; Zhang, R.; French, D.; Grigore, M.; Yu, B.; Wang, X.; Yu, J.; Zhao, S. Effects of Fly Ash Properties on Carbonation Efficiency in CO<sub>2</sub> Mineralisation. *Fuel Process. Technol.* **2019**, *188*, 79–88. [CrossRef]
18. Tian, S.; Jiang, J. Sequestration of Flue Gas CO<sub>2</sub> by Direct Gas–Solid Carbonation of Air Pollution Control System Residues. *Environ. Sci. Technol.* **2012**, *46*, 13545–13551. [CrossRef]
19. Zhang, X.; Liu, J.; Wang, Y.; Wang, Y.; Ji, L.; Yan, S. Regenerable Glycine Induces Selective Preparation of Vaterite CaCO<sub>3</sub> by Calcium Leaching and CO<sub>2</sub> Mineralization from Coal Fly Ash. *Chem. Eng. J.* **2023**, *459*, 141536. [CrossRef]
20. Eloneva, S.; Teir, S.; Salminen, J.; Fogelholm, C.J.; Zevenhoven, R. Fixation of CO<sub>2</sub> by Carbonating Calcium Derived from Blast Furnace Slag. *Energy* **2008**, *33*, 1461–1467. [CrossRef]
21. Zheng, X.; Liu, J.; Wei, Y.; Li, K.; Yu, H.; Wang, X.; Ji, L.; Yan, S. Glycine-Mediated Leaching-Mineralization Cycle for CO<sub>2</sub> Sequestration and CaCO<sub>3</sub> Production from Coal Fly Ash: Dual Functions of Glycine as a Proton Donor and Receptor. *Chem. Eng. J.* **2022**, *440*, 135900. [CrossRef]
22. Kunzler, C.; Alves, N.; Pereira, E.; Nienzowski, J.; Ligabue, R.; Einloft, S.; Dullius, J. CO<sub>2</sub> Storage with Indirect Carbonation Using Industrial Waste. *Energy Procedia* **2011**, *4*, 1010–1017. [CrossRef]
23. Kang, J.M.; Murnandari, A.; Youn, M.H.; Lee, W.; Park, K.T.; Kim, Y.E.; Kim, H.J.; Kang, S.P.; Lee, J.H.; Jeong, S.K. Energy-Efficient Chemical Regeneration of AMP Using Calcium Hydroxide for Operating Carbon Dioxide Capture Process. *Chem. Eng. J.* **2018**, *335*, 338–344. [CrossRef]
24. Li, W.; Huang, Y.; Wang, T.; Fang, M.; Li, Y. Preparation of Calcium Carbonate Nanoparticles from Waste Carbide Slag Based on CO<sub>2</sub> Mineralization. *J. Clean. Prod.* **2022**, *363*, 132463. [CrossRef]
25. Kodama, S.; Nishimoto, T.; Yamamoto, N.; Yogo, K.; Yamada, K. Development of a New PH-Swing CO<sub>2</sub> Mineralization Process with a Recyclable Reaction Solution. *Energy* **2008**, *33*, 776–784. [CrossRef]
26. Jeon, J.; Kim, M.J. CO<sub>2</sub> Storage and CaCO<sub>3</sub> Production Using Seawater and an Alkali Industrial By-Product. *Chem. Eng. J.* **2019**, *378*, 122180. [CrossRef]
27. Qin, J.; Zhang, Y.; Yi, Y.; Fang, M. Carbonation Treatment of Gasification Fly Ash from Municipal Solid Waste Using Sodium Carbonate and Sodium Bicarbonate Solutions. *Environ. Pollut.* **2022**, *299*, 118906. [CrossRef] [PubMed]
28. Kang, D.; Son, J.; Yoo, Y.; Park, S.; Huh, I.S.; Park, J. Heavy-Metal Reduction and Solidification in Municipal Solid Waste Incineration (MSWI) Fly Ash Using Water, NaOH, KOH, and NH<sub>4</sub>OH in Combination with CO<sub>2</sub> Uptake Procedure. *Chem. Eng. J.* **2020**, *380*, 122534. [CrossRef]
29. Ju, Y.; Zhang, K.; Yang, T.; Deng, D.; Qiao, J.; Wang, P.; You, Y.; Du, L.; Chen, G.; Kołodziejka, D.; et al. The Influence of a Washing Pretreatment Containing Phosphate Anions on Single-Mode Microwave-Based Detoxification of Fly Ash from Municipal Solid Waste Incinerators. *Chem. Eng. J.* **2020**, *387*, 124053. [CrossRef]
30. Deng, D.; Qiao, J.; Liu, M.; Kołodziejka, D.; Zhang, M.; Dionysiou, D.D.; Ju, Y.; Ma, J.; Chang, M.-b. Detoxification of Municipal Solid Waste Incinerator (MSWI) Fly Ash by Single-Mode Microwave (MW) Irradiation: Addition of Urea on the Degradation of Dioxin and Mechanism. *J. Hazard. Mater.* **2019**, *369*, 279–289. [CrossRef]

31. Ju, Y.; Deng, D.; Li, H.; You, Y.; Qiao, J.; Su, L.; Xing, W.; Liang, M.; Dionysiou, D.D. Rapid Detoxification of Dioxin and Simultaneous Stabilization of Targeted Heavy Metals: New Insight into a Microwave-Induced Pyrolysis of Fly Ash. *Chem. Eng. J.* **2022**, *429*, 131939. [[CrossRef](#)]
32. Chen, Q.; Luo, Z.; Hills, C.; Xue, G.; Tyrer, M. Precipitation of Heavy Metals from Wastewater Using Simulated Flue Gas: Sequent Additions of Fly Ash, Lime and Carbon Dioxide. *Water Res.* **2009**, *43*, 2605–2614. [[CrossRef](#)]
33. Wang, L.; Chen, Q.; Jamro, I.A.; Lia, R.D.; Baloch, H.A. Accelerated Co-Precipitation of Lead, Zinc and Copper by Carbon Dioxide Bubbling in Alkaline Municipal Solid Waste Incinerator (MSWI) Fly Ash Wash Water. *RSC Adv.* **2016**, *6*, 20173–20186. [[CrossRef](#)]
34. Dal Pozzo, A.; Armutlulu, A.; Rekhina, M.; Müller, C.R.; Cozzani, V. CO<sub>2</sub> Uptake Potential of Ca-Based Air Pollution Control Residues over Repeated Carbonation–Calcination Cycles. *Energy Fuels* **2018**, *32*, 5386–5395. [[CrossRef](#)]
35. Han, S.J.; Im, H.J.; Wee, J.H. Leaching and Indirect Mineral Carbonation Performance of Coal Fly Ash–Water Solution System. *Appl. Energy* **2015**, *142*, 274–282. [[CrossRef](#)]
36. Ni, P.; Xiong, Z.; Tian, C.; Li, H.; Zhao, Y.; Zhang, J.; Zheng, C. Influence of Carbonation under Oxy-Fuel Combustion Flue Gas on the Leachability of Heavy Metals in MSWI Fly Ash. *Waste Manag.* **2017**, *67*, 171–180. [[CrossRef](#)]
37. Zhu, Z.; Guo, Y.; Zhao, Y.; Zhou, T. Carbon Reclamation from Biogas Plant Flue Gas for Immobilizing Lead and Neutralizing Alkalis in Municipal Solid Waste Incineration Fly Ash. *Chem. Eng. J.* **2022**, *435*, 134812. [[CrossRef](#)]
38. Zheng, R.; Wang, Y.; Liu, Z.; Zhou, J.; Yue, Y.; Qian, G. Environmental and Economic Performances of Municipal Solid Waste Incineration Fly Ash Low-Temperature Utilization: An Integrated Hybrid Life Cycle Assessment. *J. Clean. Prod.* **2022**, *340*, 130680. [[CrossRef](#)]
39. Li, H.; Sun, J.; Gui, H.; Xia, D.; Wang, Y. Physicochemical Properties, Heavy Metal Leaching Characteristics and Reutilization Evaluations of Solid Ashes from Municipal Solid Waste Incinerator Plants. *Waste Manag.* **2022**, *138*, 49–58. [[CrossRef](#)]
40. Li, Y.; Zhang, J.; Liu, Z.; Chen, L.; Wang, Y. Harmless Treatment of Municipal Solid Waste Incinerator Fly Ash through Shaft Furnace. *Waste Manag.* **2021**, *124*, 110–117. [[CrossRef](#)]
41. Yang, Z.; Tian, S.; Ji, R.; Liu, L.; Wang, X.; Zhang, Z. Effect of Water-Washing on the Co-Removal of Chlorine and Heavy Metals in Air Pollution Control Residue from MSW Incineration. *Waste Manag.* **2017**, *68*, 221–231. [[CrossRef](#)]
42. GB8978-1996; Integrated Wastewater Discharge Standard. State Environmental Protection Agency: Beijing, China, 1996.
43. Carroll, J.J.; Slupsky, J.D.; Mather, A.E. The Solubility of Carbon Dioxide in Water at Low Pressure. *J. Phys. Chem. Ref. Data* **1991**, *20*, 1201–1209. [[CrossRef](#)]
44. Zhang, Y.; Lin, S.; Qiao, J.; Kołodyńska, D.; Ju, Y.; Zhang, M.; Cai, M.; Deng, D.; Dionysiou, D.D. Malic Acid-Enhanced Chitosan Hydrogel Beads (MCHBs) for the Removal of Cr(VI) and Cu(II) from Aqueous Solution. *Chem. Eng. J.* **2018**, *353*, 225–236. [[CrossRef](#)]
45. Zhou, N.; Luther, G.W.; Chan, C.S. Ligand Effects on Biotic and Abiotic Fe(II) Oxidation by the Microaerophile *Sideroxydans Lithotrophicus*. *Environ. Sci. Technol.* **2021**, *55*, 9362–9371. [[CrossRef](#)] [[PubMed](#)]
46. Wu, K.J.; Tse, E.C.M.; Shang, C.; Guo, Z. Nucleation and Growth in Solution Synthesis of Nanostructures—From Fundamentals to Advanced Applications. *Prog. Mater. Sci.* **2022**, *123*, 100821. [[CrossRef](#)]
47. Van Gerven, T.; Moors, J.; Dutré, V.; Vandecasteele, C. Effect of CO<sub>2</sub> on Leaching from a Cement-Stabilized MSWI Fly Ash. *Cem. Concr. Res.* **2004**, *34*, 1103–1109. [[CrossRef](#)]
48. Trushina, D.B.; Bukreeva, T.V.; Kovalchuk, M.V.; Antipina, M.N. CaCO<sub>3</sub> Vaterite Microparticles for Biomedical and Personal Care Applications. *Mater. Sci. Eng. C* **2014**, *45*, 644–658. [[CrossRef](#)] [[PubMed](#)]
49. Trushina, D.B.; Bukreeva, T.V.; Antipina, M.N. Size-Controlled Synthesis of Vaterite Calcium Carbonate by the Mixing Method: Aiming for Nanosized Particles. *Cryst. Growth Des.* **2016**, *16*, 1311–1319. [[CrossRef](#)]
50. Fernandez-Martinez, A.; Hu, Y.; Lee, B.; Jun, Y.S.; Waychunas, G.A. In Situ Determination of Interfacial Energies between Heterogeneously Nucleated CaCO<sub>3</sub> and Quartz Substrates: Thermodynamics of CO<sub>2</sub> Mineral Trapping. *Environ. Sci. Technol.* **2013**, *47*, 102–109. [[CrossRef](#)]
51. Jia, K.; Feng, Q.; Zhang, G.; Ji, W.; Zhang, W.; Yang, B. The Role of S(II) and Pb(II) in Xanthate Flotation of Smithsonite: Surface Properties and Mechanism. *Appl. Surf. Sci.* **2018**, *442*, 92–100. [[CrossRef](#)]
52. Zhang, S.; Wen, S.; Xian, Y.; Zhao, L.; Feng, Q.; Bai, S.; Han, G.; Lang, J. Lead Ion Modification and Its Enhancement for Xanthate Adsorption on Smithsonite Surface. *Appl. Surf. Sci.* **2019**, *498*, 143801. [[CrossRef](#)]
53. Chiang, K.Y.; Hu, Y.H. Water Washing Effects on Metals Emission Reduction during Municipal Solid Waste Incinerator (MSWI) Fly Ash Melting Process. *Waste Manag.* **2010**, *30*, 831–838. [[CrossRef](#)]
54. Jiang, J.; Chen, M.; Zhang, Y.; Xu, X. Pb Stabilization in Fresh Fly Ash from Municipal Solid Waste Incinerator Using Accelerated Carbonation Technology. *J. Hazard. Mater.* **2009**, *161*, 1046–1051. [[CrossRef](#)] [[PubMed](#)]
55. Ukwattage, N.L.; Ranjith, P.G.; Yellishetty, M.; Bui, H.H.; Xu, T. A Laboratory-Scale Study of the Aqueous Mineral Carbonation of Coal Fly Ash for CO<sub>2</sub> Sequestration. *J. Clean. Prod.* **2015**, *103*, 665–674. [[CrossRef](#)]
56. Liu, W.; Su, S.; Xu, K.; Chen, Q.; Xu, J.; Sun, Z.; Wang, Y.; Hu, S.; Wang, X.; Xue, Y.; et al. CO<sub>2</sub> Sequestration by Direct Gas–Solid Carbonation of Fly Ash with Steam Addition. *J. Clean. Prod.* **2018**, *178*, 98–107. [[CrossRef](#)]
57. Yuan, Q.; Yang, G.; Zhang, Y.; Wang, T.; Wang, J.; Romero, C.E. Supercritical CO<sub>2</sub> Coupled with Mechanical Force to Enhance Carbonation of Fly Ash and Heavy Metal Solidification. *Fuel* **2022**, *315*, 123154. [[CrossRef](#)]
58. Chen, J.; Lin, X.; Li, M.; Mao, T.; Li, X.; Yan, J. Heavy Metal Solidification and CO<sub>2</sub> Sequestration from MSWI Fly Ash by Calcium Carbonate Oligomer Regulation. *J. Clean. Prod.* **2022**, *359*, 132044. [[CrossRef](#)]

59. Wang, L.; Jin, Y.; Nie, Y.; Li, R. Recycling of Municipal Solid Waste Incineration Fly Ash for Ordinary Portland Cement Production: A Real-Scale Test. *Resour. Conserv. Recycl.* **2010**, *54*, 1428–1435. [[CrossRef](#)]
60. Tong, Z.; Ma, G.; Zhou, D.; Yang, G.; Peng, C. The Indirect Mineral Carbonation of Electric Arc Furnace Slag Under Microwave Irradiation. *Sci. Rep.* **2019**, *9*, 7676. [[CrossRef](#)]
61. Zhou, G.T.; Yao, Q.Z.; Fu, S.Q.; Guan, Y.B. Controlled Crystallization of Unstable Vaterite with Distinct Morphologies and Their Polymorphic Transition to Stable Calcite. *Eur. J. Mineral.* **2010**, *22*, 259–269. [[CrossRef](#)]
62. Han, Y.S.; Hadiko, G.; Fuji, M.; Takahashi, M. Factors Affecting the Phase and Morphology of CaCO<sub>3</sub> Prepared by a Bubbling Method. *J. Eur. Ceram. Soc.* **2006**, *26*, 843–847. [[CrossRef](#)]
63. Dang, H.C.; Yuan, X.; Xiao, Q.; Xiao, W.X.; Luo, Y.K.; Wang, X.L.; Song, F.; Wang, Y.Z. Facile Batch Synthesis of Porous Vaterite Microspheres for High Efficient and Fast Removal of Toxic Heavy Metal Ions. *J. Environ. Chem. Eng.* **2017**, *5*, 4505–4515. [[CrossRef](#)]
64. Lin, P.Y.; Wu, H.M.; Hsieh, S.L.; Li, J.S.; Dong, C.; Chen, C.W.; Hsieh, S. Preparation of Vaterite Calcium Carbonate Granules from Discarded Oyster Shells as an Adsorbent for Heavy Metal Ions Removal. *Chemosphere* **2020**, *254*, 126903. [[CrossRef](#)] [[PubMed](#)]
65. Liu, W.; Huang, G.; Su, X.; Li, S.; Wang, Q.; Zhao, Y.; Liu, Y.; Luo, J.; Li, Y.; Li, C.; et al. Zebrafish: A Promising Model for Evaluating the Toxicity of Carbon Dot-Based Nanomaterials. *ACS Appl. Mater. Interfaces* **2020**, *12*, 49012–49020. [[CrossRef](#)] [[PubMed](#)]

**Disclaimer/Publisher’s Note:** The statements, opinions and data contained in all publications are solely those of the individual author(s) and contributor(s) and not of MDPI and/or the editor(s). MDPI and/or the editor(s) disclaim responsibility for any injury to people or property resulting from any ideas, methods, instructions or products referred to in the content.